Nanoscale

Investigation of surface passivation mechanism through Ag-doped Al-rich film using solution processes

Journal:	*Nanoscale*
Manuscript ID	NR-ART-10-2015-006883.R1
Article Type:	Paper
Date Submitted by the Author:	20-Nov-2015

Complete List of Authors:	Khan, Firoz; DGIST, Baek, Seong-Ho; DGIST, Energy research Kim, Jae Hyun; Daegu Gyeongbuk Institute of Science & Technology (DGIST), Energy Research Division

SCHOLARONE™
Manuscripts

Please do not adjust margins

Nanoscale

ARTICLE

Investigation of surface passivation mechanism through Ag-doped Al-rich film using solution processes

Received 00th January 20xx,
Accepted 00th January 20xx

DOI: 10.1039/x0xx00000x

www.rsc.org/

Firoz Khan, Seong-Ho Baek, and Jae Hyun Kim*

Electronic recombination loss is an important issue for photovoltaic (PV) devices. While it can be reduced by using a passivating layer, most of the techniques used to prepare passivating layers are either not cost effective or not applicable for device applications. Previously, it was reported that a low cost sol-gel derived Al-rich zinc oxide (ZnO:Al) film serves as an effective passivating layer for p-type silicon but is not effective for n-type silicon. Herein, we studied the elemental composition of the film and the interfacial structure of ZnO:Al:Ag/n-Si using TEM, XPS, FTIR, and SIMS analyses. The XPS analysis revealed that Ag-rich zones randomly formed in the film near the ZnO:Al:Ag//n-Si interface, which induced a positive charge at the interface. The maximal value of effective minority carrier lifetime ($\tau_{eff} \approx 1581$ µs) is obtained for wafer using ZnO:Al:Ag passivating layer with $R_{Ag/Zn}$ = 2%. The corresponding limiting surface recombination velocity is ~ 16 cm/s. The FTIR absorption area of Si-H bonds is used to calculate the hydrogen content in the film. The hydrogen content is increased with increasing Ag content up to $R_{Ag/Zn}$ = 2% to a maximal value of 3.89 x 10^{22} atoms/cm^3 from 3.03 x 10^{22} atoms/cm^3 for $R_{Ag/Zn}$ = 0%. The positive charge induced at the interface may cause band bending, which would produce an electric field that repels the minority charge carriers from the interface to the bulk of n-Si. Two basic phenomena, chemical passivation due to Si-H bonding and field effect passivation due to the charge induced at the interface, have been observed for effective passivation of the n-Si surface. An implied V_{oc} of 688.1 mV is obtained at illumination intensity of 1 sun.

Introduction

The current trend in wafer based silicon photovoltaics (PVs) towards thinner crystalline silicon wafer to reduce the cost of the materials as well as recombination in the bulk[1]. However, surface recombination can be reduced via optimization of the properties of the surface state (suppressing the defect density using surface passivation) or by reducing the surface concentration of charge carriers of either electrons or holes using a low-high junction[2]. The surface can be passivated via bonding of a passivating layer chemically with dangling bonds at the surface (chemical passivation) or the fixed charges in the passivating layer repel the majority carriers and the extremely large fixed charges bend the energy band, resulting in an inversion layer at the surface[3]. Several techniques have been reported in the literature to passivate the silicon surfaces. Most of them either require high processing temperature or special equipment, however, and consequently are not cost effective due to their processing cost[1-3].

It has been reported that hydrogen annealed sol-gel processed Al rich ZnO (ZnO:Al) films passivate p-type silicon (p-Si) effectively[2,4]. These films also have been used as passivating layers on the back surface of bifacial solar cells[5], and for passivated emitter and rear cells (PERCs)[6]. Previously, the Al content in the ZnO:Al film has been optimized[7], and the interface properties between the passivating layer and p-Si also have been studied[8]. However, ZnO:Al does not effectively passivate n-type silicon (n-Si). We later found that a small amount of Ag-doping in a ZnO:Al film (ZnO:Al:Ag) effectively passivated n-Si surfaces[9]. Effect of Ag doping on some of the properties of air annealed ZnO:Al:Ag nanostructures have been studied in our previous work[10]. It is therefore important to study the effects of Ag doping on passivation properties of hydrogen annealed ZnO:Al:Ag film.

We investigate low cost Ag doped Al-rich ZnO films as an effective passivating layer on silicon surface first time. In this paper, we report on the effects of Ag doping on surface passivation properties of a sol-gel derived ZnO:Al:Ag film of Cz grown n-type silicon wafers. The properties of the interface between the film and n-Si and the elemental composition of the film also have been discussed.

Results and discussion

Structural and Morphological properties

In all the films, Al to Zn molar ratio ($R_{Al/Zn}$) is constant, whereas, the molar ratio of Ag to Zn ($R_{Ag/Zn}$) is varies from 0 to 3%. Henceforth, the film synthesized using the solution with

Division of Nano and Energy Convergence Research, Daegu Gyeongbuk Institute of Science & Technology (DGIST), 50-1 Sang-Ri, Hyeonpung-Myeon, Dalseong-gun, Daegu 711-873, Republic of Korea. E-mail: jaehyun@dgist.ac.kr
†Electronic Supplementary Information (ESI) available: See DOI: 10.1039/x0xx00000x

This journal is © The Royal Society of Chemistry 2015

Please do not adjust margins

$R_{Ag/Zn}$ = 0%, 1%, 2%, and 3% are referred to as ZnO:Al:Ag-0, ZnO:Al:Ag-1, ZnO:Al:Ag-2, and ZnO:Al:Ag-3, respectively. A detailed study has been made for ZnO:Al:Ag-2, which is simply referred as ZnO:Al:Ag[10].

Figure1 shows the XRD patterns of the ZnO:Al:Ag-0, ZnO:Al:Ag-1, ZnO:Al:Ag-2, and ZnO:Al:Ag-3 films coated on silicon wafers and annealed in a forming gas ambient at 500°C. In all the samples, Bragg peaks at 2θ = 31.82°, 34.46°, 36.12°, 47.6°, 56.63°, 62.88° and 68.05° are observed, corresponding to hexagonal ZnO from the (100), (002), (101), (102), (110), (103), and (112) reflection planes, respectively. The crystalline phase present in the film is identified as the wurtzite hexagonal crystal structure of ZnO (JCPDS card no: 36-1451). One additional peak corresponding to the (121) reflection plane of $H_2Al_{10}O_{16}$ is observed at 2θ = 51.5° in the ZnO:Al:Ag-0 and ZnO:Al:Ag-1 samples. Another peak at 2θ = 38.26° in ZnO:Al:Ag-1 and two additional peaks at 2θ = 38.26° and 44.53° in the ZnO:Al:Ag-2 and ZnO:Al:Ag-3 films corresponding to Ag are observed (JCPDS card no: 2-1098). One more peak corresponding to Ag_2O at 2θ = 38.05° is also observed for $R_{Ag/Zn}$ = 2% and 3% (shown in Figure S1 of supporting information). For higher Ag doping (more than 1%), the Ag reacts with oxygen of $H_2Al_{10}O_{16}$ that results formation of Ag_2O and $H_2Al_{10}O_{16}$ is disappeared.

The peak intensities corresponding to the (100) and (101) reflection planes increased with Ag doping. The poly-crystalline character of the film thus increased with an increase of Ag doping[11]. The lattice enlargement due to the ionic size difference between Ag^+ (1.26 Å) and Zn^{2+} (0.74 Å) and formation of Ag_2O may causes intensity change of ZnO peak at 2θ = 31.82°, 34.46° and 36.12°.

Figure 2 shows for surface morphology of ZnO:Al:Ag films with various Ag doping levels that are first baked at 200 °C in air and then annealed under a forming gas ambient at 500 °C. It can be noted that the Al content in all the films are very high that destroyed the crystal structure and also formed Al_2O_3 due to segregation at the grain boundaries[2,12]. Due to the size difference between Al^{3+} (0.54 Å) and Zn^{2+} (0.74 Å), the replacement of Zn^{2+} by Al^{3+} creates some vacancies in the ZnO lattice[2,12]. These vacancies are compensated by a slight doping of Ag up to the saturation level (~ 1%)[10]. For further increase in the Ag doping (more than 1%), Ag_2O is formed as shown in the Figure S1 of the supporting information. This may be the cause for formation of some amorphous regions. Notably, the ZnO:Al:Ag-2 film shows the poor crystallinity due to formation of amorphous regions and increased polycrystalline nature. This may lead to increased diffusion of hydrogen towards the interface between the film and silicon. However, for the Ag doping of 3%, more Ag_2O is formed, which destroyed the crystal structure again and ZnO:Al:Ag-3 has the micro-structure little bit similar to ZnO:Al:Ag-0. But the crystalline size of ZnO:Al:Ag-3 is higher than ZnO:Al:Ag-0. This may be due to the size difference between Ag^+ than Zn^{2+}. Owing to increase in segregation of Ag for $R_{Ag/Zn}$ = 3% at grain boundaries, the number of grain boundaries is increased and hence traps sites are also increased.

Passivation properties

Figure 3a shows the measured τ_{eff} of n-Si wafers passivated by ZnO:Al:Ag films for various $R_{Ag/Zn}$ along with bare wafer (uncoated). Previously, the Al contents in Al rich ZnO was used for passivation of p-Si optimised to achieve a maximal τ_{eff}[7]. A maximal value of τ_{eff} was obtained for $R_{Al/Zn}$ = 30%[7]. Thus, in this study, $R_{Al/Zn}$ is kept constant (30%) and optimized the value of $R_{Ag/Zn}$. The value of τ_{eff} increased to 71.1 µs from its initial value of 14.2 µs (bare silicon) after application of ZnO:Al:Ag-0. After application of the Ag-doped film, τ_{eff} further increased to 629.9 µs for $R_{Ag/Zn}$ = 1% and a maximal value of τ_{eff} was obtained for $R_{Ag/Zn}$ = 2% (1581.2 µs). Finally, it decreased to a value of 872.6 µs for $R_{Ag/Zn}$ = 3%. The decrease in the τ_{eff} for higher Ag doping (more than 2%) is attributed to the increase in the trap sites or/and appearance of metallic character of Ag[10]. The trap sites and metallic Ag works as sink for the minority charge carriers[7]. Hence, further increase in the Ag doping decreases the τ_{eff}. The corresponding surface recombination velocities (S_{eff}) are calculated using a bulk lifetime (τ_b) of 1600 µs, 2000 µs and ∞ (as shown in Fig. 3a). The calculated S_{eff} values are obtained (for τ_b = 1600 µs) as 336.5 cm/s, 24.1 cm/s, 0.2 cm/s, and 13.0 cm/s after passivation with ZnO:Al:Ag-0, ZnO:Al:Ag-1, ZnO:Al:Ag-2, and ZnO:Al:Ag-3 films, respectively from an initial value of 1744.9 cm/s for a bare wafer. The τ_{eff} values are also used to calculate maximum possible S_{eff} assuming bulk lifetime (∞) using the following relation

$$S_{eff,max} = \frac{W}{2\tau_{eff}} \quad (1)$$

where, W is the wafer thickness.

The measured τ_{eff} values (for $R_{Ag/Zn}$ = 2%) and their corresponding calculated $S_{eff,max}$ values with Δn are plotted in Fig. 3b. The obtained value $S_{eff,max}$ is ~15.81 cm/s for specified value of τ_{eff}. However, the $S_{eff,max}$ for bare wafer is ~ 1760.56 cm/s. The maximum value of τ_{eff} (1645.9 µs) is obtained at Δn = 1.5 x 10^{15} cm^{-3}, it decreases with further increase of Δn. The specified values are taken at Δn = 3.5 x 10^{15} cm^{-3}.

Atomic bonding analysis

Figure 3c shows the FTIR transmission spectra of ZnO:Al:Ag films with $R_{Ag/Zn}$ = 0% to 3% in a wavenumber range of 400-1200 cm^{-1} to investigate the bonding in the film or at the interface. Several peaks with small intensity corresponding to ZnO in a wavenumber range of 400-520 cm^{-1} are observed in all the samples[13]. One absorption peak at ~ 576 cm^{-1} corresponding to Al-O is found all the samples. On additional absorption peak at ~ 470 cm^{-1} corresponding to Ag-O is observed in the Ag doped samples (ZnO:Al:Ag-1, ZnO:Al:Ag-2, and ZnO:Al:Ag-3)[14] which is also confirmed by XRD result as shown in Figure S1 of the supporting information. A broader peak in a wavenumber range of 1077 to 1136 cm^{-1} corresponding to SiO_x is observed in all samples[15]. An important absorption peak in a range of 722-909 cm^{-1} due to the bond signature of Si-H (bending mode) is observed in all samples[15]. The area of the absorption peak corresponding to the Si-H bond is increased with an increase of Ag doping up to $R_{Ag/Zn}$ = 2%. The absorption area of the Si-H bonds is used to calculate the hydrogen content in the annealed film[16]. The

This journal is © The Royal Society of Chemistry 2015

hydrogen content increased with an increase of Ag content up to $R_{Ag/Zn}$ = 2% to a maximal value of 3.89 x 10^{22} atoms/cm^3 from 3.03 x 10^{22} atoms/cm^3 for $R_{Ag/Zn}$ = 0% (as shown in Figure 3d). However, it started to decrease with a further increase of $R_{Ag/Zn}$ and finally a value of 3.34 x 10^{22} atoms/cm^3 was obtained for $R_{Ag/Zn}$ = 3%.

Interface analysis

Figure 4(a) shows a cross-sectional HRTEM image of the ZnO:Al:Ag/n-Si structure (low magnification) to study the ZnO:Al:Ag//n-Si interface. The thickness of the ZnO:Al:Ag film is about 100 nm. At the interface, an insulating layer of SiO_x of low contrast has been formed with uniform thickness (about 3 nm). The ZnO:Al:Ag/n-Si structure gives notable results relative to the ZnO:Al//p-Si structure[8] reported in our previous study:: (i) at the ZnO:Al:Ag/n-Si interface several high contrast Ag rich zones formed; and (ii) the ZnO:Al:Ag film has a smaller d spacing value (about 0.31 nm) than the ZnO:Al film (about 0.52 nm), as shown in Figure 4(b)[8]. The TEM measurement has also done on bare Si and a very thin native SiO_x layer ~1 nm is observed[8]. This confirmed that the SiO_x layer is grown during the formation of ZnO:Al:Ag/n-Si structure at the interface due to oxidation of Si in presence of oxygen in the ZnO:Al:Ag solvent or/and ZnO lattice[8]. The selected area electron diffraction patterns (SAED) of the ZnO:Al:Ag film are shown in Figure 4(c). The ZnO:Al:Ag film is indexed similar to the ZnO:Al film (a wurtzite ZnO structure). The SAED pattern also confirmed a lower d-spacing value than the ZnO:Al film. The analysis of the SAED patterns reveals that excluding the diffraction rings of the wurtzite structure of ZnO, no additional rings are observed. Diffraction circles corresponding to (100), (002), (101), (102), (110), (103), and (112) planes of wurtzite ZnO are found[17]. Similar orientations of the reflection planes are observed in the XRD analysis.

Elemental analysis

Figure 5 shows a cross-sectional (a) STM image and elemental color mapping of (b) Ag, (c) Al, (d) Zn, (e) O, and (f) Si for an elemental analysis. It can be seen that the elemental distributions of Al, Zn, and O elements are uniform throughout the cross-section of the film. However, the distribution of Ag is not uniform. It can be also seen from color mapping of Ag that the elemental Ag density near the interface is significantly higher than in the other regions due to the high diffusion rate of Ag in the ZnO lattice[18] (as shown in Fig. 5b).

The cross-sectional line scanned (marked by arrow in Fig. 5a) EDS from the top surface of the ZnO:Al:Ag film to silicon is shown in the inset of Fig. 5a. The atomic percentages of Al, Zn, and O are ~ 17±2%, ~ 31±2%, and ~ 52±2%, respectively, whereas the atomic percentages of Ag and Si are nearly 0% and remained nearly constant up to a depth of about 80 nm. For depth beyond 80 nm, the atomic percentage of Ag started to increase and reached a maximal value of about 30% at a depth of about 98 nm (close to interface) due to the formation of an Ag rich zone. At the interface, the O atomic percentage increased slightly due to the formation of SiO_x. Ag was quantified using a XPS analysis with etching time with a step of 4 min, as shown in Fig. 6a. The XPS analysis is performed via Ar^+ ion beam sputtering with 5 keV beam energy. XPS peaks corresponding to Ag $3d_{5/2}$ and Ag $3d_{3/2}$ are observed at binding energy of 368.5 eV and 374.6 eV, respectively, after etching of 16 min. The spacing between these two peaks is 6.1 eV, which is nearly equal of Ag metal (6.0 eV)[19]. The position of Ag $3d_{5/2}$ is slightly higher than Ag metal (368.3 eV), which belongs to Ag alloy[19]. It is noteworthy that no Ag 3d peaks were observed except at an etching time of 16 min. This confirmed that the Ag ions accumulate near the interface via diffusion due to diffusion via temperature gradient. The detailed elemental scans of Al 2(p), Zn 2(p), O 1(s) and Si 2(p) with etching time are shown in Figures S2, S3, S4, and S5 of the supporting information, respectively. It shows a similar trend of elemental depth profile as obtained by EDS. The peak corresponding Al 2p spectrum is observed at 74.97 eV, which is correspond to aluminium oxide[8,19]. The detailed explanations of other element are provided elsewhere[8].

The depth profile of H content determined by SIMS is plotted in Fig. 6b. It can be seen that the H content increased very rapidly from ~ 1 x 10^5 counts at the ZnO:Al:Ag surface to 1.5 x 10^6 counts at the ZnO:Al:Ag//n-Si interface. The H diffusion rate obtained in the ZnO:Al:Ag film is substantially higher than that in the ZnO:Al films due to increase in grain boundaries up to $R_{Ag/Zn}$ = 2% (Figure 4b). This provides an easier path for H diffusion to the interface. For higher Ag doping ($R_{Ag/Zn}$ = 3%), the Ag_2O or metallic Ag block the grains that may reduce the diffusion of H[10,12]. In the ZnO:Al:Ag-3 film, the number of grain boundaries is increased and hence defect sites are increased (Figure 2d). The trapping of H atoms by these created defect (trap) sites is increased, which reduced the H content for $R_{Ag/Zn}$ = 3%. The highest value of H content is found at the interface, which may cause the formation of Si-H bonding that results in the chemical passivation of the Si surface.

Optical properties

The refractive index have also been measured in the wavelength (λ) range of 450 nm to 800 nm as shown in Figure S6 of the supporting information to evaluate the potential of these films as antireflection coating (ARC). The experimentally measured values of refractive index (μ) at λ = 600 nm of ZnO:Al:Ag films are 2.07, 1.66, 1.96, and 1.89 for $R_{Ag/Zn}$ = 0%, 1%, 2%, and 3%, respectively. This confirmed that the films with $R_{Ag/Zn}$ = 2% and 3% are very close to squire root of refractive index of silicon. Hence, these films ($R_{Ag/Zn}$ = 2% and 3%) can also be used as an effective ARC [2]. The transmittance (T) spectra of AZO thin films coated on glass substrates are shown in Figure S7 of the supporting information. The average transmittances in the 400 - 1200 nm wavelength range are found to be ~ 90 for all the films. The transmittance of all the films is nearly equal to that of uncoated glass substrate for λ > 500 nm. However, ZnO:Al:Ag-2 and ZnO:Al:Ag-3 film show significantly reduced T values (less than 80%) below λ = 390 nm and 400 nm, respectively. It indicate that these films highly transparent in the wavelength of 400 – 1200 nm (useful absorption range of solar spectrum by Si) and can be worked as good ARC on Si solar cells.

Electronic and photovoltaic properties

The physical structure and energy band diagram at equilibrium of the ZnO:Al:Ag/SiO_x/Si system are shown in Figures 7(a) and

7(b), respectively. In this structure, ZnO:Al:Ag contained partially positive charge due to the accumulation of Ag ions. Due to high Al-doping, the conductivity of the ZnO:Al:Ag film is similar to that of the ZnO:Al film, which acts as a dielectric material. Initially, Al doping may cause an increase of free charge carriers because more Al atoms are occupied at Zn lattice sites, resulting in more free charge carriers[18,20-21]. However, after a certain level of doping, no further Zn sites can be occupied by dopant atoms because of the limited solubility of Al in the ZnO crystallites[20-22]. Because the ionic radius of Al is smaller than the radius of Zn, the excess Al might occupy interstitial positions, leading to distortion of the crystal structure of ZnO, or Al atoms might also segregate at grain boundaries in the form of Al_2O_3, which would increase the grain boundary barrier[10]. The absorption edge shifted towards shorter wavelength because an increase in the carrier concentration gave rise to an increase in the band gap[20]. The E_g value decreases with an increase in Ag doping up to a certain value and then again started to increase. The narrowing of E_g is due to many body effect among charge carriers in the conduction and valence bands[23-25]. The shallow acceptor impurities create defect levels close to the valence band edge. However, the donor impurities create defect levels near the conduction band edge. Ag doping may induce impurity levels near the valence band edge of ZnO[26-28]. With a further increase in Ag doping, widening of E_g occurs due to the Burstein-Moss effect, since the highest states in the valence band are blocked and Ag starts to alloy[29]. Kelvin probe force microscopy (KPFM) has been used to investigate charge storing capacity (positive or negative) using contact potential difference (CPD) between metal tip and the samples[11,30,31]. Recently, it has been observed that a fixed positive charge is created in the ZnO:Al:Ag film near the interface[11]. When bias is applied on the sample surface, the Fermi energy level of the material is shifted due to the injection of holes (or electrons) into the sample surface. It change the contact potential value (increase or decrease) of the contact potential value[31]. Figure 7(b) shows the energy band diagram of the ZnO:Al:Ag/SiO_x/n-Si structure at thermal equilibrium. The value of the valence band maximum (VBM, E_v) and the work function (WF) or Fermi energy level (E_f) of the ZnO:Al:Ag films are determined using UPS measurement[30] (as shown in Fig 7c). The WF is calculated from the difference between energy of He I (21.2 eV) and cut-off voltage of UPS spectra. The determined WFs are 4.71 eV, 5.09 eV, 5.02 eV and 4.85 eV for $R_{Ag/Zn}$ = 0, 1, 2 and 3%, respectively. The E_f lies at 0 eV and E_v is represented by first peak at lower binding energy side (as shown in inset of Figure 7c). However, the value of the conduction band minimum (CBM, E_c) is determined by summation of E_g and E_v. E_g is determined from the absorption of the film. The obtained value of E_g for $R_{Ag/Zn}$ = 2% is ~ 3.74 eV, whereas the energy difference between E_f and E_v is 2.04 eV, as shown in Fig. 7(b). The positive charge induced at the interface may cause band bending, which would block the path of holes (minority carriers) moving from n-Si to the passivating layer and repel the minority charge carriers from the interface to the bulk of n-Si. However, holes can easily enter the n-Si from the passivating layer.

To explore the PV application, the implied open circuit voltage (V_{oc}) has been extracted from the Quasi-steady-state photoconductance (QSSPC) data using the following relation[32].

$$implied_V_{oc} = \frac{V_T(\Delta n + N_d)\Delta n}{n_i^2} \quad (2)$$

Where, V_T=kT/q, k (= 1.381 x 10^{-23} m^2kg/s^2K) is the Bolzmann's constant, q (= 1.602 x 10^{-19} C) is the electronic charge, T is the absolute temperature, N_d (= 2.78 x 10^{15} cm^{-3}) is doping density of n-Si and n_i (= 1.5 x 10^{10} cm^{-3}) is the intrinsic carrier density.

The implied V_{oc} vs. illumination intensity (P_{in}) in the P_{in} range of 0.015 to 3 suns is shown in Fig. 8. The implied V_{oc} exponentially increases with the P_{in}. The implied V_{oc} of 688.1 mV obtained at P_{in} = 1 sun. It indicates that these ZnO:Al:Ag films can be used as an effective passivating layers in PV devices.

Experimental

Synthesis of AZO Films

Ag-doped Al-rich ZnO (ZnO:Al:Ag) solution were prepared by dissolving zinc acetate dihydrate and aluminum nitrate nonahydrate in 10:3 molar ratios in ethanol, which gave a ZnO:Al solution with a 30% Al to Zn molar ratio ($R_{Al/Zn}$). A small amount of diethanolamine (DEA) was added drop wise as a stabilizer to clear the solution. Additionally, silver nitrate was added for Ag doping with an Ag to Zn molar ratio ($R_{Ag/Zn}$) of 0%, 1%, 2%, and 3%. After proper mixing by a magnetic stirrer for 4 hr at 60 °C, the solution was kept for one day at room temperature. The solution was spin-coated onto Cz grown, (100) oriented, phosphorous doped (n-type) double sided polished silicon (n-Si) wafers with ~5.0 Ω-cm resistivity, with a spinner speed of 2000 rpm. The films were allowed to dry in air for 30 min followed by initial heat treatment at 200 °C in air and finally at 500 °C under a forming gas (N_2:H_2::90:10) ambient.

Characterization techniques

X-ray diffraction (HR-XRD) patterns of the films were taken from a 2θ value 30° to 80° using a high resolution diffractometer (M/s Empyrean, Pananalytical) to evaluate the structural properties of the films. Field emission scanning electron spectroscopy (FESEM) images of films were taken for surface morphology (M/s Hitachi, S-4800). Transmittance spectra of all the films coated on glass substrates were recorded in the wavelength range of 250-1200 nm using spectrophotometer (M/s Agilent Technologies UV-Vis-NIR system, Carry-5000). The refractive index of the films were measured in the wavelength of 450-800 nm using an ellipsometer (M/s Horiba Scientific, Japan, Auto SE). X-ray photoelectron spectrometer (XPS) (M/s Thermo Scientific, ESCALAB 250Xi) measurements were performed to study the elemental composition of the passivating layer and interface using an ultrahigh vacuum setup equipped with a monochromatic Al Kα X-ray source (1486.6 eV). All the XPS peaks were calibrated using the C 1s peak. The work function

This journal is © The Royal Society of Chemistry 2015

of the ZnO:Al:Ag film was measured using a UV photoelectron spectrometer equipped with XPS using a He I ion source (21.2 eV). The work function was calibrated using an Au standard sample. Scanning transmission electron microscopy (STEM), energy dispersive x-ray spectroscopy (EDS), and high-resolution transmission electron microscopy (HRTEM) (M/s Hitachi, HF-3300/NB5000/S-4800) were used for imaging of the atomic structure of the sample in cross-sectional mode. Fourier transform infrared (FTIR) transmission spectra were recorded at room temperature using a Thermo Scientific FTIR Microscope (Model: Continuum) in a wave number range of 400-4000 cm^{-1}. The depth profile of H ions was analyzed using secondary ion mass spectrometry (SIMS) with an analysis area of 33 μm (diameter), Cs^{+} gun, impact energy of 5 keV, current of 20 nA, and raster size of 200 μm x 200 μm. The lifetime of the minority charge carriers in the silicon samples was measured using a Sinton Instrument WCT-120 lifetime tester[32]. Quasi-steady-state photoconductance (QSSPC) technique was used to determine the minority carrier lifetime as a function of injected photocarrier density (Δn) up to 1.0 x 10^{16} cm^{-3}. The QSSPC lifetime measurement also yielded the implied V_{oc} vs. P_{in}, which was comparable to an illuminated I-V curve at each stage of solar cell process in the light bias range of 0-50 suns[33]. The light intensity was calibrated with the help of silicon reference solar cell. This technique offers quick determination of photoconductivity (used for photoconductive materials and solar cell structure both) or photo-voltage (used for solar cell structure) without significant heating of the materials. The measurement of photoconductance was done by contactless method, i.e., coupling of coil in a bridge circuit[34]. For solar cell structure, both photoconductivity decay (PCD) and photo-voltage decay (PVD) are used, whereas, only PCD is used for materials. In our case, PCD technique was used for bare and passivated silicon wafers. The reported measured effective lifetime (τ_{eff}) was taken at Δn = 3.5 x 10^{15} cm^{-3}.

Conclusions

A cost effective sol-gel derived Ag-doped, Al-rich zinc oxide film for passivating layer of n-type silicon has been investigated. HR-TEM and EDS analyses confirmed that the ZnO:Al:Ag is polycrystalline with a reduced d-spacing value (~ 0.31 nm). A thin SiO_x layer with a thickness of ~ 3 nm is formed at the ZnO:Al:Ag//n-Si interface. The XPS analysis revealed that Ag rich zones randomly formed in the film near the interface, which induced a positive charge at the interface. The highest value of τ_{eff} (1581.2 μs) was obtained for the ZnO:Al:Ag passivating layer with $R_{Ag/Zn}$ = 2%, which gave the maximum S_{eff} value (~ 16 cm/s). The absorption area of Si-H bonds is used to calculate the hydrogen content in the film. The hydrogen content increased with an increase of Ag content up to $R_{Ag/Zn}$ = 2% to a maximal value of 3.89 x 10^{22} atoms/cm^3 from 3.03 x 10^{22} atoms/cm^3 for $R_{Ag/Zn}$ = 0%. The hydrogen content also increased from the surface to the interface. The positive charge induced at the interface may cause band bending, which produced an electric field that repelled the minority charge carriers from the interface to the bulk of n-Si. Two basic phenomena, chemical passivation due to Si-H bonding and field effect passivation due to charge induced at the interface, have been observed for the effective passivation of the n-Si surface. These films can be used as low cost passivating layers in silicon PV devices. An implied V_{oc} of 688.1 mV is obtained at the illumination intensity of 1 sun.

Acknowledgements

This study was carried out under the support of the DGIST R&D Program (No. 15-EN-01) funded by the Ministry of Science, ICT and Future Planning of the Korean government. Also partially funded by the Ministry of Trade, Industry & Energy (MOTIE), Korea Institute for Advancement of Technology (KIAT), Dae Gyeong Institute for Regional Program Evaluation (DGIRPE) through the Leading Industry Development for Economic Region.

Notes and references

1 J. Schmidt, A. Merkle, R. Brendel, B. Hoex, M.C.M. van de Sanden and W.M.M. Kessels, Prog. Photovolt: Res. Appl., 2008, **16,** 461.
2 F. Khan, Fabrication of Diffused Junction Crystalline Silicon Solar Cells with Texturization and Different Antireflection Coatings and Study of Their Photovoltaic Properties, Ph.D. Thesis, Jamia Millia Islamia, New Delhi, India 2012.
3 S.W. Glunz, D. Biro, S. Rein and W. Warta, J. Appl. Phys., 1999, **86,** 683.
4 F. Khan, Vandana, S.N. Singh, M.Husain and P.K. Singh, Sol. Ener. Mater. Sol. Cells, 2012, **100,** 57.
5 F. Khan, S.H. Baek, S.N. Singh, P.K. Singh and J.H. Kim, Sol. Ener., 2013, **97,** 474.
6 F. Khan, S.H. Baek, A. Mobin and J.H. Kim, Sol. Ener., 2014, **101,** 265.
7 F. Khan, S.H. Baek, S.N. Singh, P.K. Singh, M. Husain and J.H. Kim, Sol. Ener., 2014, **110,** 595.
8 F. Khan, S.H. Baek, J.H. Kim, Semicond. Sci. Technol., 2015, **30,** 015012.
9 F. Khan, S.H. Baek and J.H. Kim, Passivation of n-type silicon wafers, Korean Patent (submitted KO-10-2014-0157939).
10 F. Khan, S.H. Baek and J.H. Kim, J. Alloy. Comp., 2014, **584,** 190.
11 F. Khan, S.H. Baek, J.Y. Lee, and J.H. Kim, J. Alloy. Comp., 2015, 647, 566.
12 S.Y. Kuo, W.C. Chen, F.I. Lai, C.P. Cheng, H.C. Kuo, S.C. Wang, W.F. Hsieh, J. Cryst. Growth, 2006, 287, 78.
13 G. Xiang, U. Pal, J.G. Serrano, K.B. Ucer and R.T. Williams, Phys. Stat. Sol., 2006, **c 3,** 3577.
14 N.L. Yong, A. Ahamad and A.W. Mohammad, Int. J. Sci. Engg. Research, 2013, **4,** 155.
15 Z. Ma, K. Chen, X. Huang, J. Xu, W. Li, Y. Sui, D. Zhu, J. Mei and D. Feng, J. Appl. Phys., 2004, **95,** 2448.
16 W.A. Lanford and M.J. Rand, J. Appl. Phys., 1978, **49,** 2473.
17 R.M. Wang, Y.J. Xing, J. Xu and D.P. Yu, New J. Phys., 2003, **5,** 115.
18 G.Y. Huang, C.Y. Wang and J.T. Wang, J. Phys.: Condens. Matter, 2009, **21,** 345802.
19 J.F. Moulder, W.F. Stikel, P.E. Sobol and K.D. Bomben, Hand Book of X-Ray Photoelectron Spectroscopy: A Reference Book of Standard Spectra for Identification and Interpretation of XPS Data (Eden Prairie, MN: Physical Electronics), 1995.
20 D. Iqbal, A. Kostka, A. Bashir, A. Sarfraz, Y. Chen, A.D. Wieck and A. Erbe, ACS Appl. Mater. Interface, 2014, **6,** 18728.

This journal is © The Royal Society of Chemistry 2015

21 D.G. Baik and S.M. Cha, Thin Solid Films, 1999, **354,** 227.
22 J.H. Lee and B.O. Park, Thin Solid Films, 2003, **426,** 94.
23 K.F. Berggren and B.E. Sernelius, Phys. Rev. B, 1981, **24,** 1971.
24 E. Burstein, Phys. Rev., 1954, **93,** 632.
25 B.E. Sernelius, Phys. Rev. B, 1987, **36,** 4878.
26 A.Y. Oral, Z.B. Bahsi, M.H. Aslan, Appl. Surf. Sci., 2007, **253,** 4593.
27 Y. Cao, L. Miao, S. Tanemura, M. Tanemura, Y. Kuno and Y. Hayashi, Appl. Phys. Lett., 2006, **88,** 251116.
28 S. Ilican, M. Caglar and Y. Caglar, Appl. Surf. Sci., 2010, **256,** 7204.
29 B.E. Sernelius, K.F. Berggren, Z.C. Jin, I. Hamberg, C.G. Granqvist, Phys. Rev., B 1988, **37,** 10244.
30 A. Kumar, T.S. Herng, K. Zeng and J. Ding, ACS Appl. Mater. Interface, 2012, **4,** 5276.
31 M.F. Wong, T.S. Herng, Z.K. Zhang, K.Y. Zeng and J. Ding, Appl. Phys. Lett., 2010, **97,** 232103.
32 R.A. Sinton and A. Cuevas, Appl. Phys. Lett., 1996**, 69,** 2510.
33 http://www.sintoninstruments.com/PDFs/Sinton-Instruments-WCT-120-product-note.pdf
34 T. Pisarkiewicz, Opto-Electron. Rev., 2004, **12,** 33.

This journal is © The Royal Society of Chemistry 2015

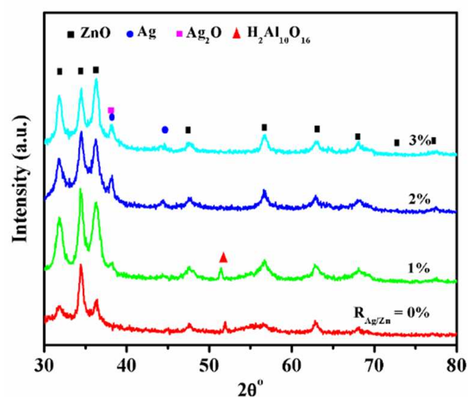

Figure 1. XRD spectra of ZnO:Al:Ag film coated on n-Si and annealed in forming gas.

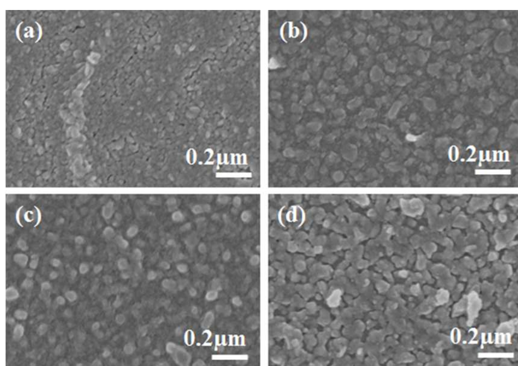

Figure 2. FESEM images of ZnO:Al:Ag films with $R_{Ag/Zn}$ = **(a)** 0%, **(b)** 1%, **(c)**, 2%, and **(d)** 3%.

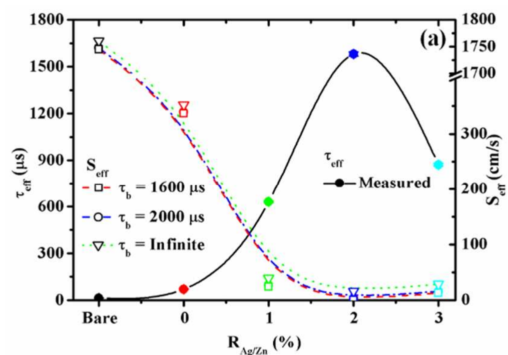

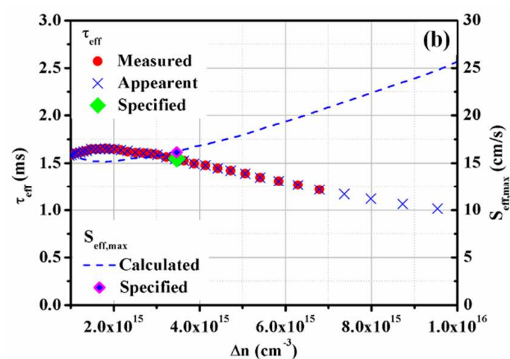

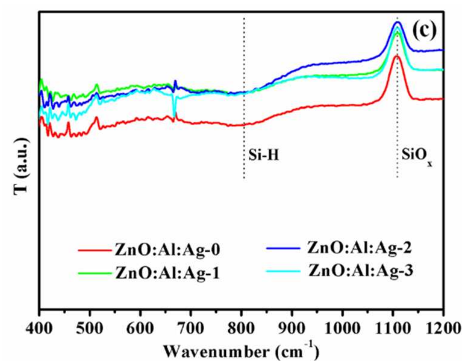

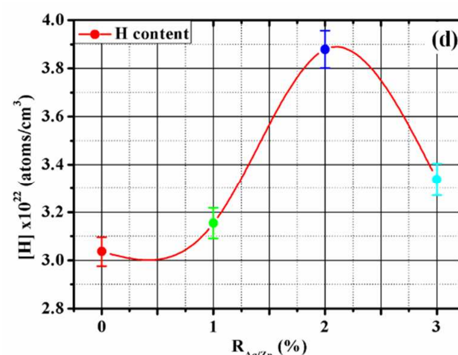

Figure 3. **(a)** Measured τ_{eff} along with calculated S_{eff} (for τ_b = 1600μs, 2000μs and ∞) of n-Si vs. $R_{Ag/Zn}$, **(b)** Measured τ_{eff} along with calculated S_{eff} vs. Δn, **(c)** FTIR transmittance spectra of forming gas annealed ZnO:Al:Ag films for various Ag-doping coated on Si in a wavenumber range of 400 – 1200 cm^{-1}, and **(d)** Hydrogen content vs. $R_{Ag/Zn}$ determined from the absorption peak FTIR spectra corresponding to Si-H bonding.

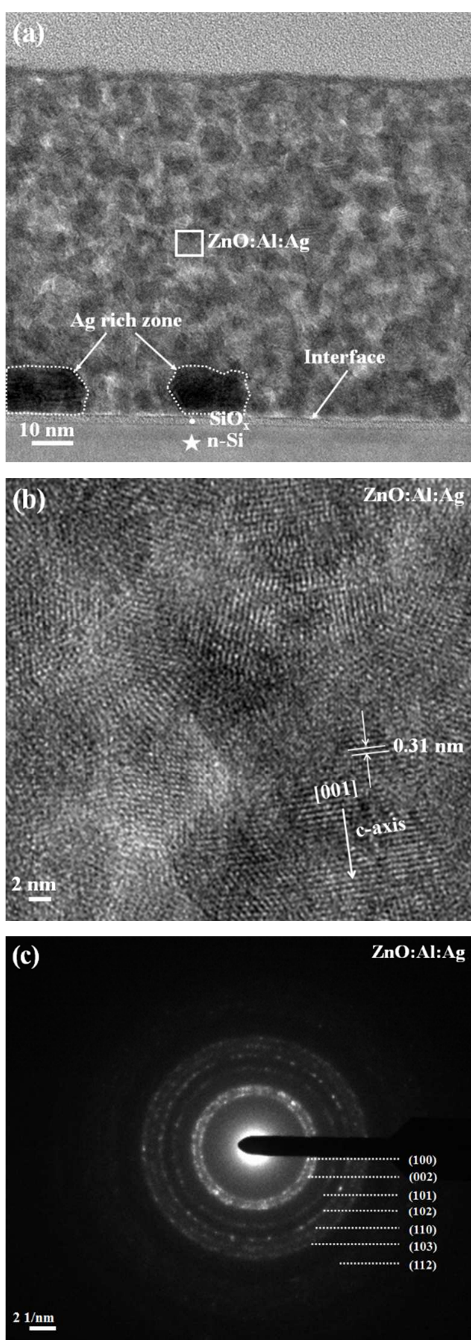

Figure 4. Analytical TEM investigations of ZnO:Al:Ag/n-Si structure **(a)** cross-sectional HR-TEM image with low magnification, **(b)** cross-sectional HR-TEM image of ZnO:Al:Ag film with high magnification, and **(c)** SAED pattern of ZnO:Al:Ag film.

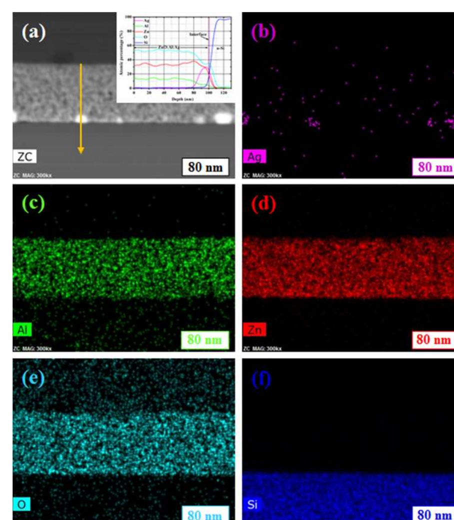

Figure 5. Cross-sectional view of (a) STEM image (in inset depth profile using line EDS scan corresponding to arrow marked) of elements and elemental EDS color mapping of (b) Ag, (c) Al, (d) Zn, (e) O, and (f) Si.

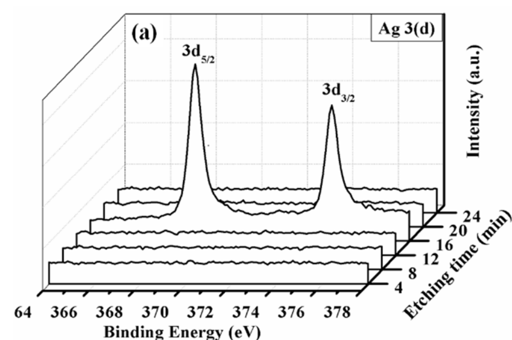

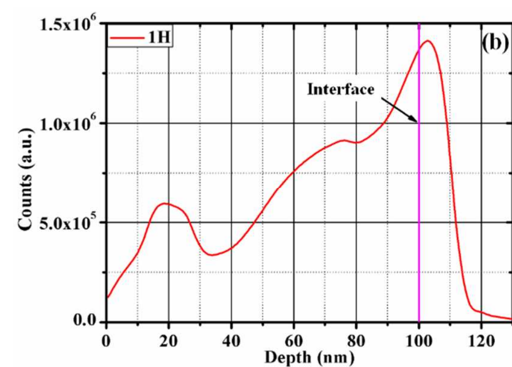

Figure 6(a) XPS spectra of montage display of Ag 3(d) peak with etching time using sputtering (Ar^+) from ZnO:Al:Ag-2 surface to n-Si, **(b)** Hydrogen depth profile in the ZnO:Al:Ag/SiO_x/n-Si structure using a SIMS measurement.

This journal is © The Royal Society of Chemistry 2015

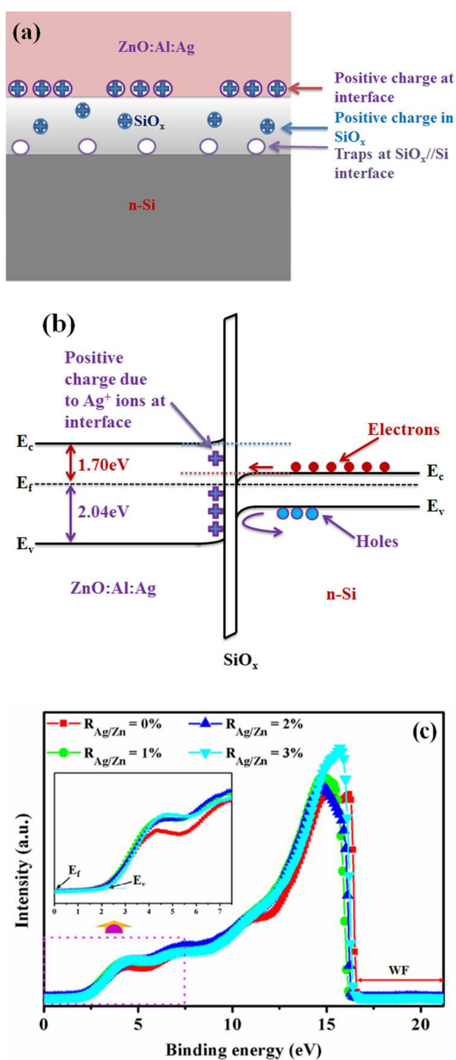

Figure 7(a) Physical structure of ZnO:Al:Ag/SiO_x/n-Si structure for charge/trap distribution, **(b)** energy band diagram at equilibrium of ZnO:Al:Ag/SiO_x/n-Si system, and **(c)** UPS measurement results for ZnO:Al:Ag samples. The Fermi level (E_f) of all the samples lies at 0 eV and first peak at lower BE represents the position of valence band maximum (E_v) as shown in inset.

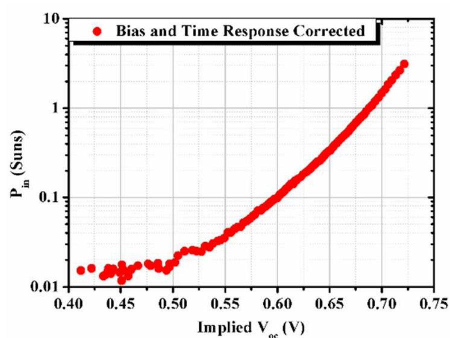

Figure 8 Implied V_{oc} vs. illumination intensity.